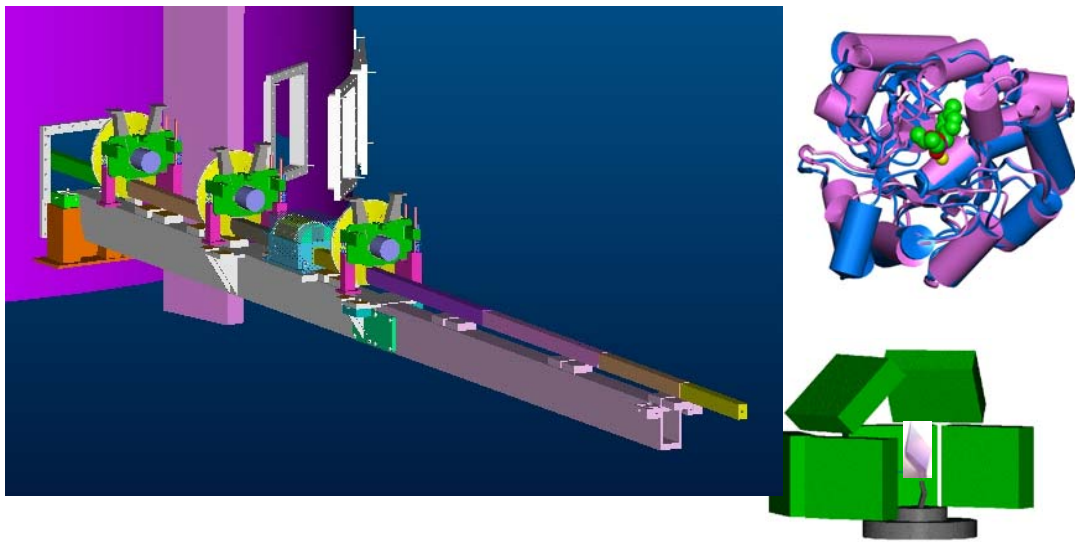


Letter of Intent

“MANDI”

Macromolecular Neutron Diffractometer
at the
Spallation Neutron Source



Spokespersons:

A. Mesecar – UIC (mesecar@uic.edu)

A. J. Schultz – IPNS, ANL (ajschultz@anl.gov)

P. Thiyagarajan – IPNS, ANL (thiyaga@anl.gov)



Acknowledgement

The IDT acknowledges the financial assistance of Oak Ridge Associated Universities (ORAU) for support of Christine Rehm, SNS, who performed the Monte Carlo simulations of the instrument. We also wish to thank Jason Hodges, SNS, for his expert input in the design.

Table Of Contents

1) OBJECTIVE	1
2) DESIGN CRITERIA	1
3) INTRODUCTION	2
4) SCIENTIFIC EXAMPLES	7
4.1 A. Mesecar and B. Santarsiero	9
4.1.1 <i>Isocitrate Dehydrogenase</i>	9
4.1.2 <i>Trihydroxytoluene Dioxygenase</i>	10
4.2 G. Bunick, L. Hanson, G. Petsko and D. Ringe	12
<i>Determining the mechanism for hydrogen transfer in D-Xylose Isomerase</i>	
4.3 P. Thiyagarajan, A.J. Schultz, P. Laible, D.K. Hanson and R. Pokkaluri	15
<i>Determination of hydrogen atoms and bound water molecules in photosynthetic reaction center complex</i>	
5) INSTRUMENT DESIGN	16
5.1 Layout of MANDI	16
5.2 Moderator choice	19
5.2.1 Resolution with different moderators	20
5.2.2 Effective FWHM of the pulses	21
5.2.3 Coupled hydrogen, $L = 75.5$ m	23
5.2.4 Choice based on counting statistics	24
5.2.5 Conclusion on moderator choice	25
6) EFFECTIVE FLUX	25
7) RESOLUTION	26
8) DESIGN CALCULATIONS USING MC SIMULATIONS	28
9) BEAM DEFINING OPTICS AT THE SAMPLE	31
10) DETECTORS	31
11) EXPECTED PERFORMANCE OF MANDI	32
12) POLARIZATION OPTICS FOR BACKGROUND REDUCTION	34
13) PRELIMINARY BUDGET	34
14) REFERENCES	34
15) IDT MEMBERS AND THEIR AFFILIATION	38

LETTER OF INTENT

MANDI: Macromolecular Neutron Diffractometer at the Spallation Neutron Source

1) OBJECTIVE

Neutron macromolecular crystallography (NMC) has the unique ability to provide the precise positions of hydrogen atoms and bound water molecules in biological macromolecules. In order to exploit the high neutron flux that will become available by 2006 at the Spallation Neutron Source (SNS), and to leverage the enormous interest shown by the macromolecular crystallography community, we propose to develop a dedicated best-in-class high throughput and high resolution time-of-flight single crystal neutron macromolecular crystallography diffractometer (MANDI) at the SNS high power target station (HPTS). A decoupled liquid hydrogen moderator at the SNS is the appropriate source for this high resolution diffractometer from the point of view of both the flux and pulse width. We therefore propose to build MANDI on beam line 11 where a wide shutter will effectively provide full view of the moderator for both MANDI on beam line 11B and POW-GEN3 on beam line 11A.

2) DESIGN CRITERIA

MANDI will be designed to be the best-in-class for fast and efficient measurements of a set of Bragg data with a resolution of 1.5 Å on macromolecular crystals with lattice constants in the range of 150 Å ($\Delta d/d = 1\%$). Instrument design will take advantage of the opportunities presently available during the SNS construction phase for the complete optimization of the instrument. For a given resolution it will achieve the highest throughput, minimal peak overlap and high signal-to-noise ratio by using a large wavelength bandwidth of neutrons sorted by time-of-flight (TOF) and an array of high spatial resolution position-sensitive area detectors covering a large solid angle. Reduction in radiation damage to the biological samples by γ rays and high energy neutrons will be accomplished by the use of curved guides to make the sample out of the line-of-sight of the moderator. Choppers will be used to provide access to different wavelength bands. Furthermore, flexibility will exist to match the flux, angular divergence, and consequently instrument resolution to different experimental requirements.

3) INTRODUCTION

NMC can fill an important niche in structural biology¹⁻²³ and functional genomics that even ultra high resolution macromolecular X-ray crystallography (UHRMXC) at synchrotrons cannot adequately fulfill. Although UHRMXC at third generation X-ray synchrotrons can locate the positions of protons in cases where highly ordered crystals are available, in many instances the structural information obtained for solvation shells and protonation states at critical sites of the enzymes continues to remain inadequate, even when working at cryo-temperatures. Enzymologists, molecular biologists and protein crystallographers are seeking complementary techniques that can provide accurate information on the positions of the protons and water molecules at active sites of enzymes in order to elucidate the mechanistic details involved in their function.

During the past few years, there have been major advances in neutron macromolecular crystallography.^{1,10-18} It has been demonstrated that NMC can provide accurate hydrogen positions even at a moderate 2.0 to 2.4 Å resolution at room temperature.^{11,12} The large difference in the neutron scattering cross-sections of hydrogen and deuterium nuclei has been exploited to extract important structural information on exchangeable protons and bound water in macromolecules.^{6,10} Crystals of deuterated proteins have shown enhanced visibility of hydrogen atoms in the neutron crystallographic data.¹⁴ Since long wavelength neutrons do not cause any radiation damage to macromolecular crystals, experiments were carried out at room temperature from which more hydrogen atoms were localized than could be achieved by UHRMXC conducted at cryo-temperatures.

There is no doubt that synchrotron X-rays will continue to remain as the major tool for the structural analysis of macromolecules. The role of NMC will be to resolve the positions of hydrogen atoms at the active sites, the protonation states of certain moieties and the locations of bound water molecules. The pioneering work of Wlodawer and Hendrickson¹⁹ clearly demonstrated that the simultaneous refinement of the data from NMC and X-ray macromolecular crystallography (XMC) results in more information content than either type of data alone. The complementarity of XMC and NMC has been exploited in several studies including bovine pancreas trypsin inhibitor,²⁰ ribonuclease A:uridine vanadate complex,²¹ and insulin.²² Recent studies by Helliwell's group^{23,24} on the sugar binding protein concanavalin A have clearly shown the power of using both NMC and UHRMXC²⁴ in resolving more bound water molecules than

with UHRMXC alone. For instance, the NMC study of concanavalin A²³ revealed the positions of over 62 bound D₂O molecules when compared to only 12 H₂O molecules by UHRXMC²⁴. A study of the complex of aspartic proteinase endothiasepsin²⁵ resolved the positions of crucial protons and buried negatively charged carboxylated groups, both of which were not observed by the XMC. Another outstanding example is the study of cyclodextrin inclusion complexes by Saenger and Steiner,²⁶ wherein dynamically disordered networks of conventional and non-conventional hydrogen bonds (C-H...O, C-H... π) were observed. It is likely that such hydrogen bonds may be important in the structure-function relationship of many membrane protein structures near the hydrophobic/polar interfaces.

Another area where NMC has a potential to make a strong impact is the structural biology of the membrane proteins. Although there have been enormous achievements in solving the crystal structures of aqueous proteins [over 20,000 total entries in the Protein Data Bank (PDB)], only a handful of membrane proteins (26 entries in the PDB) have been solved to date despite the fact that about 40% of the genome consists of membrane bound proteins. One obvious reason for this limited success is the difficulty in growing suitable crystals of membrane proteins. However, when the crystallization effort does succeed, the radiation damage with X-rays becomes another road block for structure analysis. It is likely that NMC will serve as a versatile tool in advancing this important field of structural biology.

With such unique attributes, one would expect that NMC would have already made substantial contributions to structural biology. However, a survey of the literature indicates that the overall contribution has so far been limited. The reasons for the limited impact include the lack of powerful instruments dedicated to macromolecular crystallography and intrinsic flux limitation at the current facilities. In contrast to the numerous X-ray macromolecular crystallography facilities across the world, at present there are only four instruments that are recognized to be useful for single crystal neutron macromolecular crystallography: D19 and LADI at the Institut Laue-Langevin (ILL), Grenoble, France; BIX3 at the Japan Atomic Energy Research Institute (JAERI); and PCS at Los Alamos National Laboratory. While LADI and BIX3 were operational during the past 3 to 5 years, the time-of-flight diffractometer PCS has become available only recently. Thus the field of NMC has been severely constrained by the lack of dedicated instruments.

The advent of the Spallation Neutron Source (SNS) at Oak Ridge National Laboratory offers an excellent opportunity for the development of a powerful diffractometer for NMC applications. Since SNS is a new source that is still under construction, a great deal of flexibility exists now for building a fully optimized diffractometer for NMC.

Recognizing the unique information obtainable with NMC, enzymologists and macromolecular crystallographers are indicating strong interest in a dedicated neutron macromolecular crystallography diffractometer at the SNS. On December 18-19, 2000, a workshop, co-sponsored by the SNS project and the National Aeronautics and Space Administration (NASA), was held in Knoxville to discuss the future use of the SNS for macromolecular single crystal neutron diffraction. This workshop brought together representatives of both the structural biology community using X-rays and neutrons and the microgravity crystal growth community. At the conclusion of the workshop, the following recommendations were made:

- Single crystal biological instrumentation should form an integral part of the SNS instrument suite.
- All funding options should be pursued and supported to facilitate the development of two instruments for neutron macromolecular crystallography studies at SNS.
- On behalf of the group, the workshop organizers should submit a letter of intent to the Experimental Facilities Advisory Committee (EFAC), proposing macromolecular diffraction instruments both at the Long Wavelength Target Station (LWTS) and the High Power Target Station (HPTS).

Following the workshop recommendation, Professor Chris Dealwis, University of Tennessee, Knoxville, presented a scientific case to EFAC wherein he discussed the lack of structural information on crucial protons and bound water molecules that play important roles in several enzyme catalysis reactions, and the need for a dedicated neutron diffractometer for macromolecular crystallography. Although EFAC responded positively, the project did not immediately progress further.

Since SNS construction has been progressing well, and scientists from other fields have been working hard proposing (and securing funding) for an increasing number of spectrometers at the SNS, structural biologists have recognized that a window of opportunity to build a dedicated macromolecular diffractometer would close unless immediate steps are taken to put

forward a proposal to build an instrument at SNS. On May 28, 2002, at the American Crystallographic Association meeting in San Antonio, a Steering Committee including scientific personnel with expertise in protein crystallography, enzymology, and neutron instrumentation, was formed to look into the requirement of a dedicated diffractometer at the SNS. The Steering Committee members in alphabetical order are Gerry Bunick (ORNL), Chris Dealwis (University of Tennessee), Leif Hanson (University of Tennessee), Thomas Koetzle (BNL), Andrew Mesecar (University of Illinois, Chicago), Arthur Schultz (ANL), P. Thiyagarajan (ANL), and Jinkui Zhao (SNS). During the scientific talks and poster presentations at the ACA meeting, the committee members identified several scientific cases that can benefit from NMC. Steering Committee members recognized that many scientists were not aware of the construction of the SNS and the versatility of neutrons in providing the key information on hydrogen atom positions that they are seeking. However, when told about the advantages provided by NMC, many expressed overwhelming support for the development of a high throughput dedicated diffractometer at SNS. An email survey conducted during September 2002 also showed tremendous interest for such an instrument. The Steering Committee accordingly adopted two action items:

- To hold focused workshops bringing the scientific community together to discuss the scientific problems that would greatly benefit from NMC and to form an instrument development team (IDT);
- To showcase the science using neutron protein crystallography at the Transactions Symposium at the 2003 ACA annual meeting in Cincinnati.

Efforts to address both action items are underway. It was also decided that the time is ripe to present an updated scientific case to the EFAC highlighting the current scientific landscape in structural and functional biology. During the October 2002 EFAC meeting, Professor Andrew Mesecar, University of Illinois, Chicago, presented a talk highlighting several scientific problems in the area of enzymology where NMC can provide unique structural information on crucial hydrogen atoms that UHRXMC does not provide. Arthur Schultz, IPNS, presented a talk on the design aspects of a macromolecular diffractometer at the SNS. Based on these presentations EFAC responded positively with the following recommendations:

- A very strong case made by Mesecar for protein crystallography;

- Decide on right trade-off in resolution and flux at SNS for highest information access rate;
- Possibility to gain operating experience with the planned SCD machine;
- Ultimately SNS must make an impact in protein crystallography;
- Attention needed that lab space can support protein work.

The positive response of the EFAC and the strong interest by the structural biology community prompted us to go forward and submit this letter-of-intent (LOI) to the March 2003 EFAC meeting proposing to build a best-in-class instrument for NMC. Under the leadership of P. Thiyagarajan and Arthur Schultz, who have expertise in the design, development and operation of TOF neutron scattering instrumentation, a design project was initiated at IPNS to carry out calculations on the design of MANDI with the assistance of Christine Rehm and Jason Hodges. A grant from Oak Ridge Associated Universities (ORAU) and the SNS provided a few months of support for C. Rehm and for a design engineer, as well as funding to conduct a workshop to bring together the scientists interested in NMC.

An instrument development team (IDT) was organized earlier this year with the goal to design, build and finally operate a dedicated time-of-flight diffractometer, MANDI, for the neutron macromolecular crystallography studies at SNS. By using well established analytical procedures and Monte Carlo simulations we carefully analyzed the performance of MANDI at both the coupled and decoupled liquid hydrogen moderators. Details of our calculations are given in a later section. Our calculations show that MANDI will perform better at a decoupled liquid hydrogen moderator that produces a high flux of cold neutrons with $\lambda = 1.5 \text{ \AA}$ to 5 \AA , and with narrow pulse widths. We became aware that the beam line 11, which views the above moderator, has a wide shutter that can readily provide full access to another instrument, in addition to POW-GEN3 at position 11A. An instrument that uses cold neutrons in combination with a curved guide to steer the beam so that the sample is out of line-of-sight is ideal for this beam line. Such a configuration fits very well with the requirements of the MANDI instrument and hence we propose to EFAC to reserve beam line 11B for this instrument.

Design calculations indicate that MANDI can gain a number of advantages by using state-of-the-art high index neutron supermirror guides:

- The flux at the sample position in MANDI can be increased by over a factor of 10.

- When compared to a “no guide” instrument that views the full moderator area (9 cm x 8 cm at 6 m), the instrument with a guide has a much smaller guide entrance area (1.5 cm x 1.5 cm) which helps to reduce the instrument background.
- The use of the guides offers flexibility to optimize the flux and angular resolution at the sample depending on the resolution requirements of a given experiment.
- A curved guide in the middle section greatly reduces the radiation damage by γ rays and high energy neutrons to the biological samples, and a straight guide following a curved guide enables beam homogenization.

Selection of the wavelength band can be accomplished by using a set of 3 choppers at appropriate locations. MANDI will employ a kappa orienter and several high resolution (1 mm) position-sensitive area scintillation detectors covering a large solid angle. With a unique combination of solid angle coverage and a wide bandwidth of neutron wavelengths, it is expected that MANDI will outperform the present world class reactor instrument BIX3 at JAERI by a factor of 50.

When MANDI becomes operational during 2007 it will be the best in the world for the single crystal NMC in providing the highest data rates and resolution. Based on its potential to serve a large scientific community of structural biologists specializing in structural genomics, proteomics and enzymology, the IDT will seek to secure funding for the design, construction and operation of MANDI.

4) SCIENTIFIC EXAMPLES

Many of the enzymes and proteins of current scientific interest due to controversies surrounding their mechanisms involving proton or hydride transfer, have unit cell edge dimensions between 100 Å and 150 Å. An example of proteins and enzymes of current scientific interest to some of the IDT members is shown in Table 1.

Table 1. Examples of proteins proposed for neutron diffraction studies by some IDT members using MANDI

Protein	IDT Members	X-Ray Res (Å)	Space Group	a (Å)	b (Å)	c (Å)	β	Year	Ref.
Isocitrate Dehydrogenase	Mesecar Santarsiero	1.4 to 1.9	P4 ₃ 2 ₁ 2	103.9	103.9	150		1997-2000 and UnPub	27-30
Trihydroxytoluene Dioxygenase	Mesecar Santarsiero	1.2 to 1.5	C2	130	80	76	111	UnPub	
Phosphotriesterase	Mesecar Santarsiero	1.7-1.9	P3 ₁ 21	61	61	207		UnPub	
Enolase	Mesecar Santarsiero	1.8	C2	121.9	73.2	93.9	93.3	1996	31
D-Xylose Isomerase	Bunick Hanson Petsko Ringe	0.86	I2 2 2	94	100	104		UnPub	
Aminopeptidase	Petsko Ringe	1.20	P6 ₁ 22	108.4	108.4	93.5		2002	32
Aldose-1-epimerase	Petsko Ringe	1.40	P2 ₁ 2 ₁ 2 ₁	128	132	101		UnPub	
Alcohol Dehydrogenase	Ramaswamy Plapp	1.13	P1	44.3	51.4	92.7	103 $\alpha=88.8^\circ$ $\gamma=111.6^\circ$	2003	33,34
TEM-1 β -Lactamase	Shoichet	0.85	P2 ₁ 2 ₁ 2 ₁	41.3	61.6	89.2		2002	35
Photosynthetic Reaction Center	Thiyagarajan Schultz D. Hanson Laible Pokkaluri	2.7	P3 ₁ 21	141.4	141.4	187.2		2002	36
Amicyanin	Sukumar Thiyagarajan Davidson Mathews	1.39	P2 ₁	28.9	56.5	27.55	96.38	1993 2001	37-39
Azurin		1.9	P2 ₁	43.25	50.65	54.60	107.79	1998	

A quick scan of the unit cell dimensions in Table 1 shows that the enzyme systems of interest to the IDT members have in general at least one unit cell edge length beyond 90 Å, and in most cases beyond 100 Å. Most if not all of the enzyme systems listed in Table 1 can produce crystals with volumes greater than of 0.8 mm³, and all produce crystals that diffract beyond the 2.0 Å, the limit necessary to resolve hydrogen atoms.

4.1 A. Mesecar and B. Santarsiero

We are currently developing a number of enzyme systems for time-resolved Laue X-ray diffraction and neutron diffraction studies. Two of our model enzyme systems are isocitrate dehydrogenase (IDH) and trihydroxytoluene dioxygenase (THT-DO).

4.1.1 Isocitrate Dehydrogenase

The proposed reaction cycle for isocitrate dehydrogenase is shown in Figure 1. The reaction cycle is completed in approximately five steps (I- V) and involves the transfer of a number of putative, solvent derived protons (blue hydrogens) via a proton shuttle relay. From deuterium solvent kinetic isotope effects ($^D V_{\max} \sim 4$), we predict that at least two protons are in flight during the transition state. From a series of high-resolution X-ray crystallographic studies,^{27,28,30} we have determined that a solvent molecule is involved in a relay mechanism with Lysine230 and Aspartate283. However, we have yet to establish the protonation states,

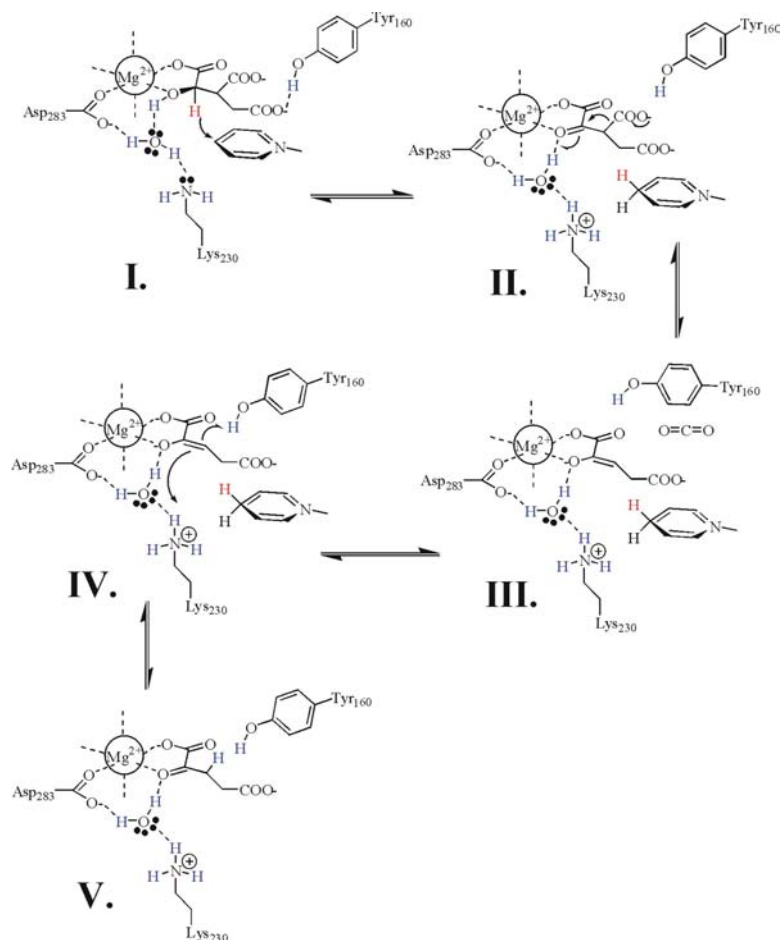


Figure 1. Putative catalytic cycle for isocitrate dehydrogenase.

hydrogen positions of isocitrate, the active site amino acid residues or the water molecule involved in catalysis. Our current hypothesis is that in the first part of the reaction cycle (I-II) Lysine230 is atypically deprotonated at neutral pH so that it acts as a base and accept protons from the hydroxyl group of the substrate via the water molecule. Once Lysine230 is protonated, it may serve as an acid to transfer a proton to the enolate intermediate (IV) that forms immediately after decarboxylation (II-III). A second possibility is that the enolate (IV) could be protonated by the mobile amino acid residue Tyrosine160. We wish to determine the neutron structures of the substrate and product bound states (I and V) in addition to the enolate bound state (III). We have synthesized a potent enolate analog that binds tightly to the enzyme form of IDH illustrated in (III),⁴⁰ and we have determined the structure of this intermediate to 1.7 Å (A. Mesecar, unpublished). Despite the fact that we are able to routinely determine 1.4 Å to 2.1 Å X-ray structures of IDH in a variety of complexes, we are still uncertain as to the positions of the hydrogen atoms. Since the reaction scheme of this enzyme potentially involves an atypical shuttle mechanism with an abnormally deprotonated lysine residue, we deem it necessary and important to pursue neutron diffraction studies to correctly establish or refute such a mechanism.

Isocitrate dehydrogenase crystals can be routinely grown between 0.8 mm-1.2 mm in the longest dimension with square bipyramidal geometry (0.5 mm to 0.7 mm) in the other dimensions. The crystals grow in the high symmetry tetragonal space group (P4₃2₁2) with dimensions of a = b = 103 Å and c = 150 Å and one molecule in the asymmetric unit. The crystals are catalytically active and they can withstand prolonged exposure to monochromatic and polychromatic synchrotron X-rays.^{29,30,41,42}

4.1.2 Trihydroxytoluene Dioxygenase

One of the most crucial reactions in the biodegradation of aromatic hydrocarbons involves the cleavage of aromatic carbon-carbon bonds. Aromatic ring-cleaving reactions are catalyzed by a class of enzymes known as non-heme metal(II) dioxygenases. These enzymes favor aromatic compounds that contain two vicinal hydroxyl groups (catechols) as substrates. Extradiol dioxygenases catalyze ring fission at bonds adjacent to one of the two hydroxyl groups. We are in the process of investigating the kinetic, chemical, and structural aspects of THTDO. To elucidate the mechanistic details of this proximal extradiol ring-cleaving enzyme, we have

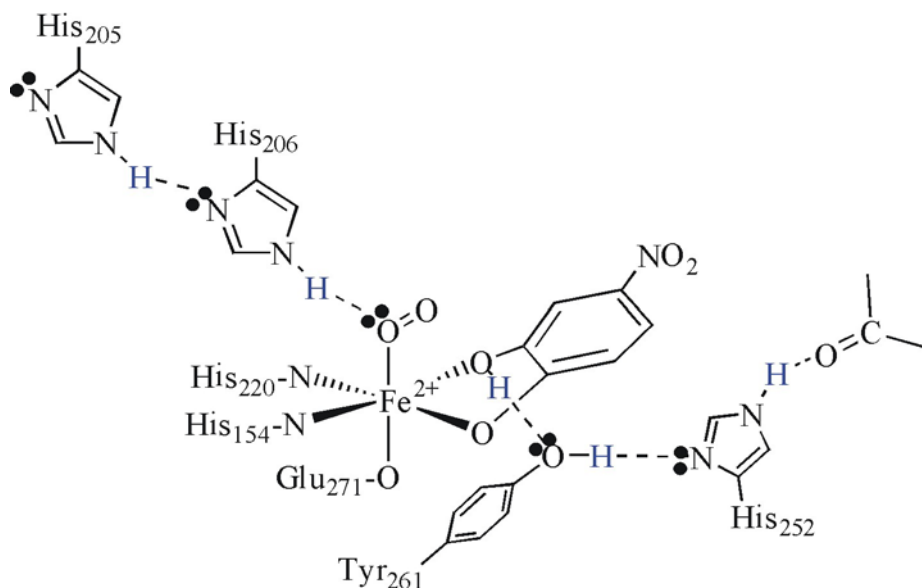


Figure 2. Putative Catalytic Cycle for Trihydroxytoluene dioxygenase.

determined the high-resolution X-ray crystal structures of native THTDO to 1.4 Å and the enzyme complexed with 4-nitrocatechol (4NC), a potent inhibitor of THTDO, to 1.2 Å. The most notable difference between the two active sites is a lengthening of the Fe-O (water, trans to Glutamate271) bond from 2.08(2) Å in the native structure to 2.58(2) Å in the 4NC structure; this is the putative site for dioxygen binding. Examination of the active sites in these high-resolution structures suggests a modification of the currently accepted mechanism for extradiol enzymes. While it is generally proposed that the involvement of a single base (Histidine206) is necessary for catalysis, we propose that this Histidine206 acts instead as an *acid*, and that the base is more probably assigned as Tyrosine261 that is activated via a proton shuttle with Histidine252 (see Figure 2). The protons involved in acid and base catalysis and the associated proton relays are shown in blue.

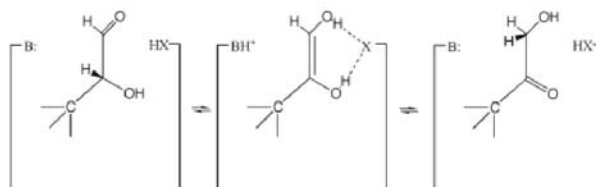
Both structures crystallize in space group C2 with moderate unit cell parameters ($a = 129$ Å, $b = 80$ Å, $c = 75$ Å). The active site is composed of a mononuclear iron atom coordinated to His154, His220, and Glu271. The octahedral coordination around the iron atom is completed by water, catechol, acetate, or other oxo-ligands. It is crucial to determine the protonation state of the active site residues and ligands. We have been able to grow relatively large crystals (400-900 microns) that diffract well beyond 1.2 Å and are very stable.

We believe that we have two interesting model enzyme systems that function via proton relay mechanisms utilizing amino acids with atypical pKa values. Neutron diffraction is one of the most powerful techniques that can be utilized to help us establish the correct mechanisms for these enzymes, despite the wealth of structural information that we already have from monochromatic and Laue X-ray structures.

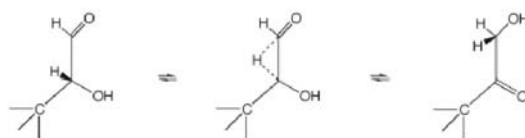
4.2 G. Bunick, L. Hanson, G. Petsko and D. Ringe

Determining the Mechanism for Hydrogen Transfer in D-Xylose Isomerase

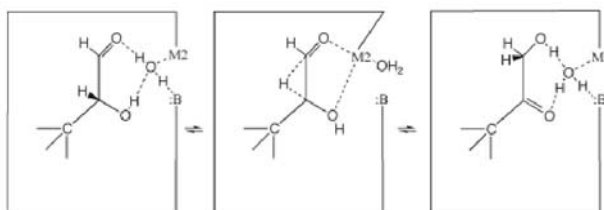
D-xylose isomerase (XI) catalyzes the conversion of D-xylose to D-xylulose and D-glucose to D-fructose by transferring a hydrogen atom from one carbon atom to an adjacent carbon atom in a sugar molecule. XI has significant commercial impact in the production of high-fructose corn syrup, but, more importantly, it serves as a model for biochemical structure and function studies of metalloenzymes. These enzymes comprise nearly one-third of all known proteins. They have significant implications in all cellular functions and in disease states such as



1.) base-catalyzed proton transfer, cis enediol intermediate



2.) hydride shift



3.) metal-ion assisted hydride shift

Figure 3. Three possible mechanisms of D-Xylose isomerase.

cancer. Three possible mechanisms have been proposed for the transfer of the hydrogen atom within the sugar substrate (Figure 3). However, despite years of intense scrutiny using atomic-resolution X-ray diffraction, a conclusive determination of the mechanism that initiates hydrogen transfer in this enzyme is still needed.

The XI enzyme binds two divalent metal ions (M1 and M2) 4.9 Å apart. Magnesium is the metal ion normally found in this enzyme, but divalent manganese or cobalt can also bind to give an active enzyme. Both of these metal ions can be replaced by certain other cations without total loss of enzymatic activity. The mode of action of this enzyme currently appears to involve an attack on the substrate by a hydrogen ion from a water molecule bound to the second metal ion, (M2). A histidine group acts as a base that assists in opening the sugar ring system in the initial stages of the mechanism. The proposed mechanisms involve a *cis* ene-diol intermediate,⁴³ a hydride-shift mechanism,^{44,45} or a hydride shift mediated by the metal ions.⁴⁶ The mechanism with a *cis* ene-diol intermediate is analogous to that in other enzymes catalyzing the same reaction but lacking metal ions. The hydride-shift mechanism involves a transfer of the hydrogen atom without any intervention from neighboring side chains in the active site. The metal ion-assisted hydride-shift mechanism includes some movement of the M2 metal ion. A second site for this metal ion has been observed in some crystal-structure determinations.⁴⁷ The binding of substrates and inhibitors to XI has also been studied by X-ray crystallographic

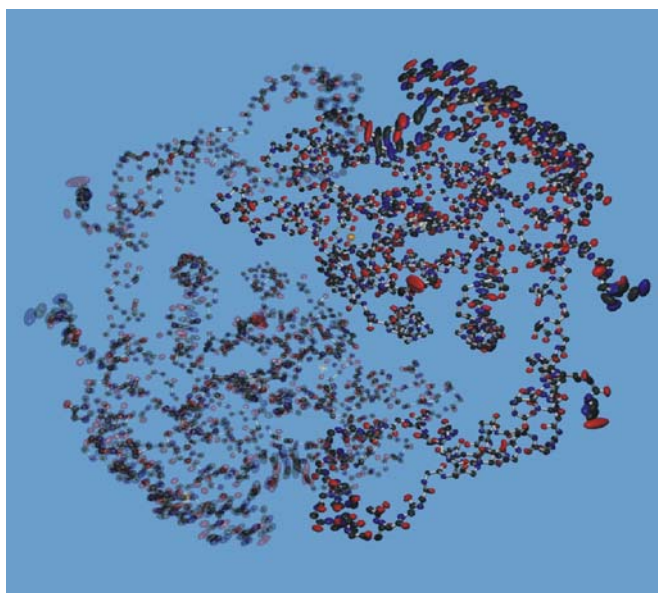


Figure 4. Overall structure of D-xylose isomerase at 0.86 Å resolution showing anisotropic B-factors on one monomer (Ringe and Petsko, unpublished data).

techniques.⁴⁸ Several different binding modes were identified. However, despite the wealth of X-ray diffraction studies and the recent ultra-high resolution 0.86 Å X-ray structure determined by Petsko and Ringe (Figure 4), the catalytic mechanism of hydrogen atom transfer has yet to be established.

Preliminary results from the neutron diffraction data recently obtained by G. Bunick and L. Hanson at the time-of-flight neutron diffractometer PCS on a large D-xylose isomerase (XI) crystal demonstrate the versatility and efficiency of the TOF technique. Figure 5 shows that the diffraction data measured using neutrons with wavelengths 1 Å to 5 Å extend to about 1.4 Å resolution with an excellent signal-to-noise ratio.

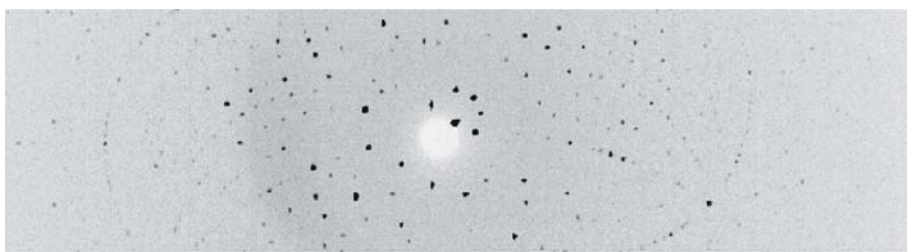


Figure 5. A Pseudo-Laue image showing Bragg reflections from D-xylose isomerase at the LANSCE PCS.

The neutron density map calculated using the diffraction data between 5 Å and 2.5 Å resolution is shown in Figure 6 for a slice of neutron density for residues 220-222. From the density map it is possible to discern that deuterium atoms have replaced ionizable hydrogen

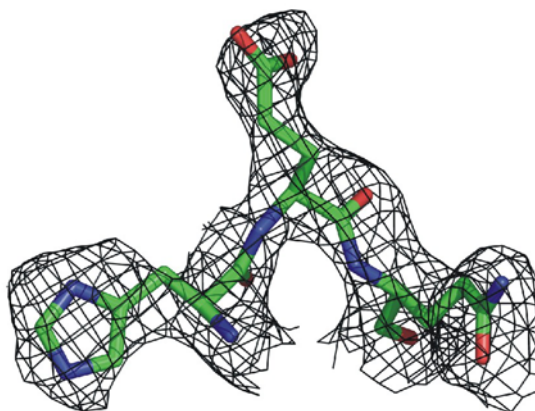


Figure 6. A slice of neutron density encompassing residues 220-222 is shown from the first Fourier transform using the neutron structure factors for XI and the 1xib X-ray coordinates.

atoms in many locations.

Since the flux is over an order of magnitude higher at the SNS than that at LANSCE, the fully optimized MANDI instrument will provide unprecedented data rates and resolution.

4.3 P. Thiyagarajan, A. J. Schultz, P. Laible, D. K. Hanson and R. Pokkaluri **Determination of Hydrogen Atoms and Bound Water Molecules in** **Photosynthetic Reaction Center Complex**

The bacterial photosynthetic reaction center (RC) was the first membrane protein for which the three dimensional structure was solved by X-ray diffraction,⁴⁹ and a Nobel Prize was awarded for this accomplishment. Since then, the structures of several mutant and wild-type RCs have been solved at resolutions ≥ 2.1 Å. This three subunit, pigment-protein complex continues to serve as an excellent model for the understanding of protein-mediated electron and proton transfer reactions. The detailed mechanisms of these reactions in the native RC have been extensively investigated by a variety of experimental techniques.⁵⁰⁻⁵⁴ These studies suggest that water molecules play an important role in the proton delivery pathways. However, obtaining their positions from X-ray diffraction data has not been successful. In order to understand the reactions involved in the electron transfer in RC, it is essential to have information on the positions of protons and bound water molecules in the RC complex.

Recently, crystals of native RCs and mutants thereof from *Rhodobacter sphaeroides* were successfully grown at ANL (Protein Engineering Group, Biosciences Division) for room temperature X-ray diffraction experiments. Methods have been developed to grow larger RC crystals (typically 0.3 mm in each dimension and a limited number with sizes up to 0.8 mm in each dimension). These crystals are grown by vapor diffusion method using concentrated RC solution in phosphate buffer containing 0.09% LDAO, 4.2% dioxane and 7.35% heptanetriol. The crystals belong to the trigonal space group (P3₁21) with unit cell dimensions of $a = b = 141.4$ Å, $c = 187.2$ Å. Although these large crystals have greatly contributed to the success of room temperature X-ray diffraction experiments, their large size most likely hinders cryo-protection attempts.

The three dimensional structure of the RC was determined from these crystals to 2.7 Å at room temperature using a laboratory X-ray source.³⁶ However, we were unable to obtain a higher resolution structure using X-ray diffraction at the Advanced Photon Source (APS)

because diffraction quality was lost when the crystals were cooled to cryogenic temperatures. Several groups have encountered problems in preserving the quality of the RC crystals when attempting to cool them to cryogenic temperatures.³⁶ So far the highest resolution that was obtained for the RC crystals at cryogenic temperatures is no better than 2.6 Å.

Since NMC has been shown to reveal the positions of hydrogen atoms even at moderate resolution, these larger crystals grown in our lab⁵⁵ should be well-suited for neutron diffraction experiments. We propose to solve the three dimensional structure of photosynthetic reaction center complex using neutron crystallography. The neutron diffraction data will be analyzed for the positions of hydrogen atoms and bound water molecules in a combined analysis with the crystal structure from X-ray diffraction data.

It is expected that the atomic resolution structure of the bacterial photosynthetic reaction center will shed light on the structural basis for efficient electron and proton transfer reactions in this integral membrane pigment-protein complex. In particular, neutron diffraction experiments will reveal functional relationships within the highly interactive network of ionizable residues and water molecules that accomplish efficient intra-protein proton delivery to reduce electron acceptors embedded within the trans-membrane portion of the protein complex.

5) INSTRUMENT DESIGN

5.1 Layout of MANDI

The layout of an optimized high throughput and high resolution MANDI instrument determined from analytical calculations and Monte Carlo simulations is shown in Figure 7, and the instrumental parameters are compiled in Table 2. As shown in Figure 7, we propose to construct the MANDI instrument on beam line 11B, which views a decoupled liquid hydrogen moderator. The moderator-to-detector length of 24.5 m of the instrument has been chosen to utilize a large wavelength band of neutrons ($\Delta\lambda = 2.69$ Å) that can be sorted by time-of-flight with a reasonable time resolution. It will use high index curved and straight guides for the efficient beam transport of cold neutrons, and bandwidth choppers to define the wavelength band for the experiments. A kappa goniometer on a positioning table will be used for mounting and orienting the crystals. A variety of beam defining optical components will be used to optimize the beam size and divergence at the sample position. An array of high resolution (1 mm spatial resolution) detectors will be used to cover a wide solid angle.

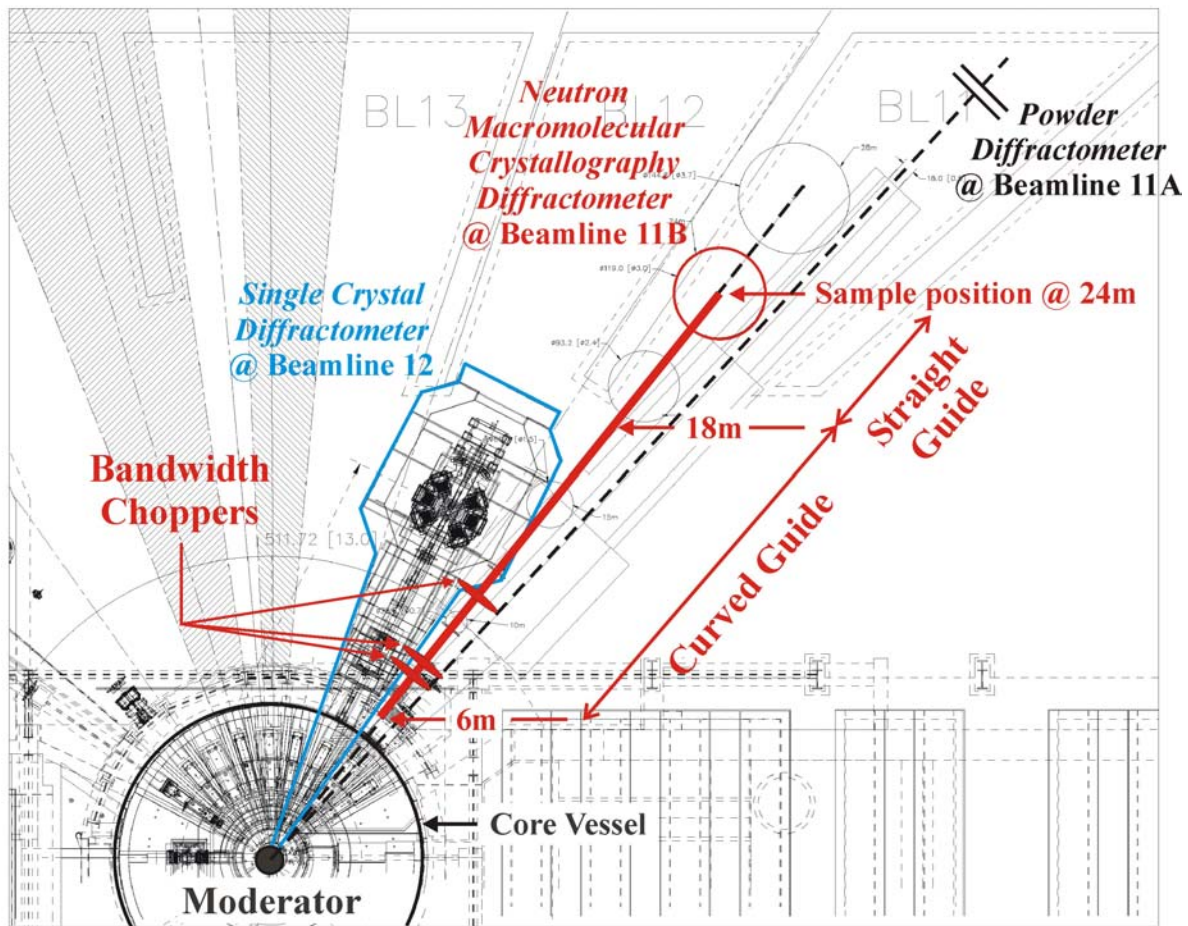


Figure 7. Layout of the MANDI instrument.

Table 2. Instrument parameters of MANDI

Moderator	Moderator type	Top Upstream
	Material	Para-Hydrogen
	Decoupler	Cadmium
	Poison	Gadolinium
	Poison depth	27 mm
	Width	0.10 m
	Height	0.12 m
Curved Guide	Starting point	6 m downstream
	Width	1.5 cm
	Height	1.5 cm
	Length	12 m
	Supermirror coating	$m > 2$
	Total turn angle	0.43°
	Radius of curvature	1599 m
	Line-of-sight lost	≈ 20 m
Straight Guide	Starting point	18 m downstream
	Width	1.5 cm
	Height	1.5 cm
	Length	5+ m
	Supermirror coating	$m > 2$
Bandwidth Choppers	Positions	7.2 m, 8.2 m, 10.4 m
Moderator-to-sample distance		24 m
Wavelength range	$2.0 \text{ \AA} \leq \lambda \leq 4.69 \text{ \AA}$	$\Delta\lambda = 2.69 \text{ \AA}$
Wavelength resolution		$\approx 0.15\%$
Natural beam divergence	vertical	0.28° (FWHM) / (std. 0.08°)
	horizontal	0.24° (FWHM) / (std. 0.07°)
Natural neutron intensity	uncollimated beam (full moderator view)	7.7×10^6 n/s
Sample Orienter	Kappa Goniometer	
Sample-to-detector distance		0.5 m
Detectors	Array of 2-D PSDs	

5.2 Moderator Choice

It has been suggested^{56,57} that a coupled moderator should be used for the NMC applications since NMC is a highly flux limited technique. Hence we propose to rigorously analyze the best moderator at SNS for MANDI. The pulse shapes for 2.55 Å neutrons from the coupled and decoupled hydrogen moderators are shown in Fig. 8. The coupled moderator will provide a peak height that is about 50% greater than the decoupled moderator, and an integrated peak intensity that is 8 times greater. This is at the expense of a much broader peak with a very long tail. MANDI is proposed for beam line 11B which views the decoupled hydrogen moderator, so we need to ask: Is the decoupled moderator suitable or better for the macromolecular diffractometer even though the coupled moderator has a much greater integrated intensity? This question has been addressed based on the resolution and signal-to-background requirements for NMC applications.

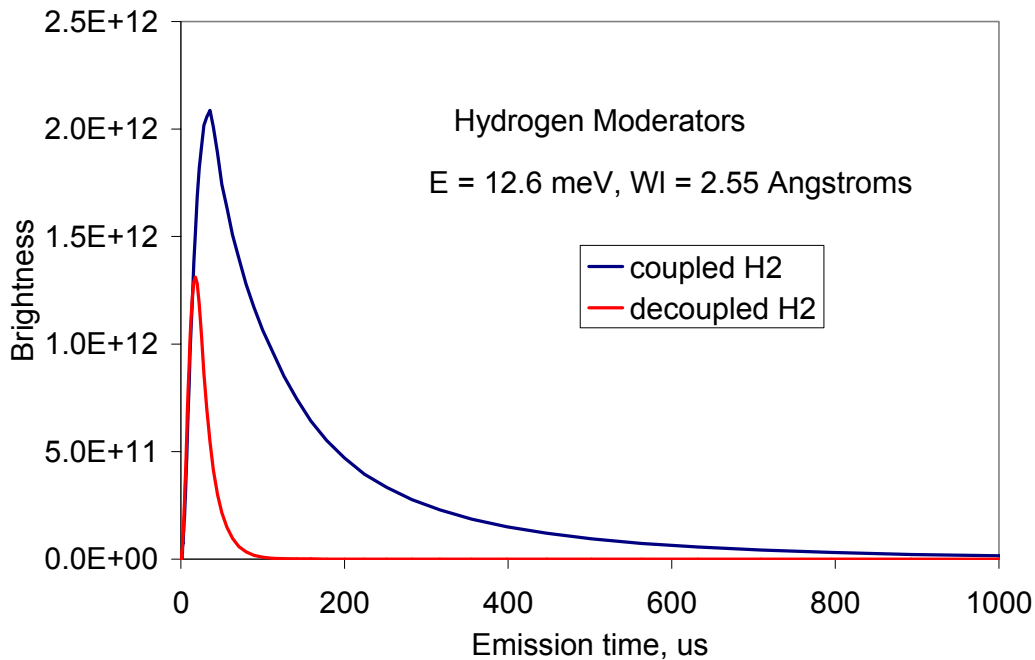


Figure 8. Emission time for neutrons with $\lambda = 2.55 \text{ \AA}$ for the coupled and decoupled liquid hydrogen moderator at the HPTS at SNS.

5.2.1 Resolution with Different Moderators

Resolution in macromolecular crystallography refers to a minimum d -spacing (d_{\min}) to which observed data are obtained (Q_{\max}), which is also related to the ability to resolve features in the structure in real space. Equation (1) describes the Q resolution of a diffractometer that depends on the pulse width of the moderator (Δt) at a given wavelength, uncertainty in the flight path length (ΔL) and angular dispersion ($\Delta 2\theta$).

$$R = \frac{\Delta Q}{Q} = \frac{\Delta d}{d} = \left[\left(\frac{\Delta t}{t} \right)^2 + \left(\frac{\Delta L}{L} \right)^2 + \left(\frac{1}{2} \Delta 2\theta \cot \theta \right)^2 \right]^{1/2} \quad (1)$$

While $\Delta L/L$ will be quite small, the other two terms dominate in determining the resolution of the instrument. Although the angular dispersion term decreases drastically with increasing scattering angle, the pulse width Δt increases with increasing wavelength, such that $\Delta t/t = \Delta\lambda/\lambda$ is ideally a constant for the range of wavelengths being used. High throughput at a given resolution can be achieved by similar but low contributions from Δt and $\Delta 2\theta$ to ΔQ , when the high flux region of the spectrum is used.

For a cubic unit cell with unit cell dimensions of $a = b = c$, it can be shown that to resolve two Bragg peaks at d_{\min} the condition in Equation (2) has to be fulfilled.

$$R < \frac{d_{\min}}{a} \quad (2)$$

The resolution R as derived from Equation (1) is based on a Gaussian distribution. For single crystal diffraction, it is not sufficient to resolve peaks, but to be able to integrate the intensity under the peak. Therefore, the peaks have to be fully separated such that the resolution requirement is^{56,57}

$$R < \frac{d_{\min}}{5a} \quad (3)$$

since from -2.5σ to $+2.5\sigma$ about the mean contains almost 99% of a Gaussian peak. The delta terms in (1) are $FWHM$ and hence

$$R_{FWHM} < \frac{d_{\min}}{2.3a} \quad (4)$$

The pulse width time resolution contributes primarily to the resolution parallel to the diffraction vector, whereas the angular resolution primarily contributes to that in the perpendicular direction.

Therefore, it can be shown that to resolve two peaks at a minimum d -spacing, d_{\min} (Å), for a cubic lattice with a lattice constant a (Å), the maximum allowable pulse length (μsec) is

$$\Delta t_{\text{pulse}}(FWHM) \leq 238.1L\left(\frac{d_{\min}^2}{a}\right)\sin\theta \quad (5)$$

where L (m) is the total path length and θ is the Bragg angle.

5.2.2 Effective FWHM of the Pulses

From Figure 8 it can be seen that the pulse shapes are not Gaussian so that $2.13FWHM$ does not contain 99% of the peak. Figure 9 displays the emission spectrum of the pulse corresponding to $\lambda = 2.55$ Å for the decoupled, poisoned parahydrogen moderator for beam line 11. The FWHM of 24.6 μsec is represented by the horizontal red line. Multiplying by 2.13, which is the equivalent of 5σ , gives what should be the full width for a Gaussian of 52 μsec (blue arrow). At this point, the intensity is about 15% of the peak maximum. For a true Gaussian at $\pm 2.5\sigma$, the intensity should be 1.7% of the maximum, which we will round off to 2%. This occurs at about 85 μsec (green arrow) for the data shown in Figure 9. The ratio of 85/52 is 1.6. Thus, we should multiply the FWHM by 1.6 to obtain an “effective FWHM” for Equation (5).

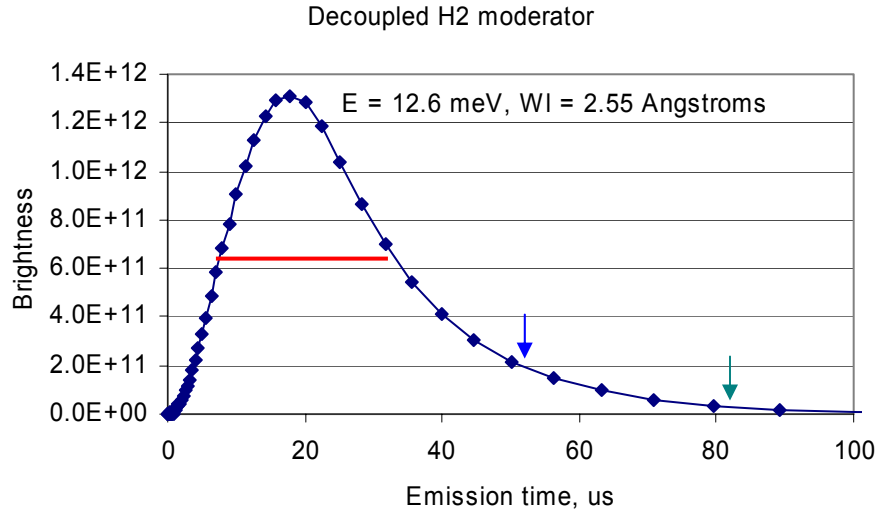


Figure 9. Emission time of neutrons with $\lambda=2.55$ Å for the decoupled H2 moderator.

For comparison, let us do a similar examination of the coupled parahydrogen moderator. At $\lambda = 2.55$ Å, the total intensity is 3.84×10^{13} n/ster/pulse/eV for the decoupled moderator, and $3.06 \times$

10^{14} n/ster/pulse/eV for the coupled moderator. Thus, the intensity of the coupled moderator for this wavelength is 8 times greater than the decoupled moderator. Figure 10 displays a pulse for

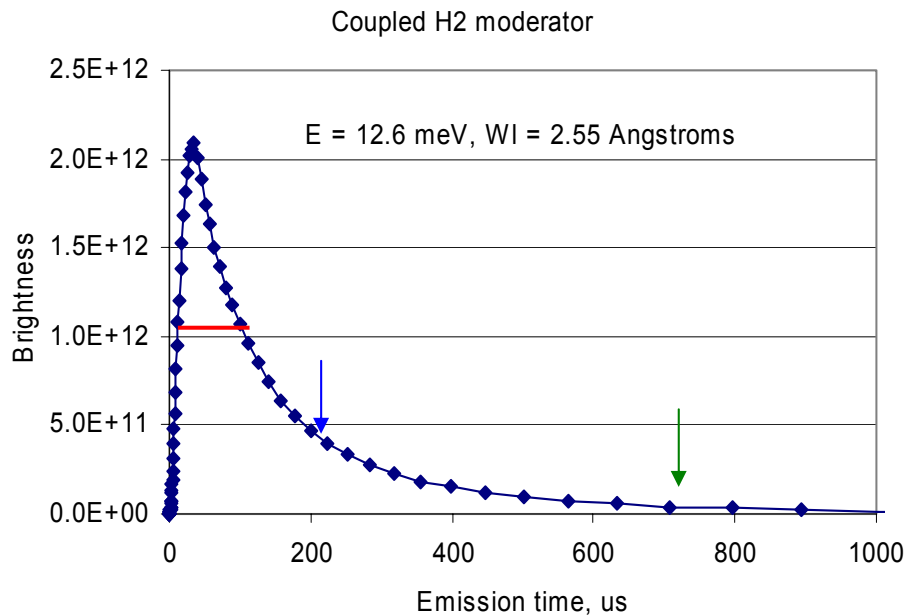


Figure 10. Emission time of neutrons with $\lambda=2.55 \text{ \AA}$ for the coupled H₂ moderator.

the coupled parahydrogen moderator at $\lambda = 2.55 \text{ \AA}$. The FWHM is 90.6 μsec and the Gaussian full width should be $2.13 \times 90.6 = 193 \mu\text{sec}$ (blue arrow), where the intensity is still 24% of the peak. The 2% intensity is achieved at 725 μsec (green arrow). Thus, the effective FWHM multiplier for the coupled moderator is $725/193 = 3.8$.

Table 3. Comparison of coupled H₂ and decoupled H₂ moderators for the pulse corresponding to $\lambda = 2.55 \text{ \AA}$

Parameter	Coupled H ₂	Decoupled H ₂	Ratio
Total intensity (n/ster/pulse/eV)	3.06×10^{14}	3.84×10^{13}	8.0
FWHM (μsec)	90.6	24.6	3.7
2% peak maximum (μsec)	725	85	8.5
Effective FWHM multiplier	3.8	1.6	2.4
Effective FWHM (μsec)	344	39	8.8

The values for the coupled and decoupled parahydrogen moderators are tabulated and compared in Table 3. In summary, although there is a potential gain of a factor 8.0 in intensity, resolution is reduced by a factor of 8.8.

Table 4 provides the minimum pulse widths from Equation (5) for resolving peaks for a cubic system with $a = 150 \text{ \AA}$, $d_{\min} = 1.5 \text{ \AA}$, and $L = 24.5 \text{ m}$ along with the “effective FWHM” for the coupled and decoupled moderators.

Table 4. Effective pulse widths vs. maximum allowed pulse lengths (Eq. 5).

2θ (deg)	λ (\AA)	Eq. (5) μsec	Dec. H2 * 1.6 μsec	Cpld. H2 * 3.8 μsec
30	0.776	23	10	36
60	1.500	44	18	71
90	2.121	62	28	193
120	2.598	76	38	364
150	2.898	85	45	397

From Table 4 the following conclusions can be made:

- The pulse width of the decoupled moderator is more than adequate at all scattering angles and wavelengths. Perhaps a partially coupled moderator or one with a greater poison depth could be useful, but such a moderator is not currently available at the SNS.
- The effective FWHM values for the coupled moderator are higher than the values in Equation (5) and in principle not useable for a 24.5 m long instrument.

5.2.3 Coupled Hydrogen, $L = 75.5 \text{ m}$

One way to use the higher flux from the coupled moderator for NMC is by increasing the flight path [see Equation (5)]. In Table 5 we provide a case for a 75.5 m flight path. It is clear that the minimum required pulse widths from Equation (5) for the present case have increased when compared to those in Table 4. The effective FWHM values of the coupled moderator are less than the values from Equation (5) only up to $2\theta = 90^\circ$.

Table 5. Maximum allowed pulse lengths [Equation (5)] vs. effective pulse widths for a 75.5 m instrument

Two-theta (deg)	WI (Å)	Eq. (5) microsec	cpld H2 microsec	cpld H2 * 3.8 Microsec
30	0.776	70	9	36
60	1.500	135	19	71
90	2.121	191	51	193
120	2.598	234	96	364
150	2.898	260	105	397

Although such a long flight path instrument can be useful for NMC applications, there are several disadvantages.

- Although the coupled moderator is 8 times more intense than the decoupled moderator, the bandwidth will decrease by a factor of 3. This reduces the maximum possible gain to 2.7.
- Total guide efficiency for longer wavelengths at 75 m may be about 60% (based on MC simulations) and much less for shorter wavelengths. So the gain may decrease to 1.6 or less.
- There is a large cost difference in constructing a 75.5 m instrument vs. a 24.5 m instrument.

5.2.4 Choice Based on Counting Statistics

For protein crystals, the large unit cells lead to weak average peak intensities. In addition, there is a high background due to the incoherent scattering from hydrogen atoms (unless the entire protein is deuterated). Because the signal-to-background ratio is small, the standard deviation of an integrated peak $\sigma(I)$ based on counting statistics is essentially the square root of the background counts B . Increasing the integrated flux by a factor of 8 gives

$$\frac{I_c}{\sigma(I_c)} = \frac{8I_d}{(8B_d)^{1/2}} = 2.8 \frac{I_d}{\sigma(I_d)} \quad (6)$$

where I_c is the Bragg peak integrated intensity with the coupled moderator and I_d is the intensity with the decoupled moderator. Thus, there would appear to be a 2.8 times improvement in signal-to-noise ratio.

However, this is only the case if the peak widths are the same, so that the number of points (time channels) that are sampled is identical. From the previous discussion of pulse widths and effective FWHM values, it is clear that anywhere from 3 to 8 times as many time channels would need to be sampled to integrate the Bragg peak with the coupled moderator. In Equation (6), increasing the background counts B by another factor of 8 essentially cancels the effective increase in the signal due to a larger flux.

5.2.5 Conclusion on Moderator Choice

Based on the superior pulse resolution of the decoupled moderator and the minimal advantage in overall counting statistics of the coupled moderator, we have concluded that the decoupled hydrogen moderator is the best choice for MANDI.

6) EFFECTIVE FLUX

We would like to evaluate an “effective flux” which is the flux multiplied by a “reflectivity” term in order to make decisions on the optimal moderator and wavelength range.

The integrated intensities I_{hkl} are reduced to structure factor amplitudes $|F_{hkl}|$ based on the Laue formula:

$$I_{hkl} = \phi(\lambda) \frac{V_s}{V_c^2} |F_{hkl}|^2 \frac{\lambda^4}{2 \sin^2 \theta} \quad (7)$$

where $\phi(\lambda)$ is the incident neutron intensity per unit wavelength range at wavelength λ ($\text{n}\cdot\text{cm}^{-2}\cdot\text{sec}^{-1}\cdot\text{\AA}^{-1}$), V_s is the sample volume, V_c is the crystal unit cell volume, F_{hkl} is the structure factor, and θ is the Bragg angle. Terms for the detector efficiency, sample absorption and extinction have not been included.

Equation (7) can be rewritten as

$$I_{hkl} = \phi(\lambda) \frac{V_s}{V_c^2} |F_{hkl}|^2 \lambda^2 d_{hkl}^2 \quad (8)$$

This leads to an effective flux of

$$\phi_{\text{eff}}(\lambda) = \phi(\lambda) \cdot \lambda^2 \quad (9)$$

In this case, one takes into account that for any hkl , the d -spacing is constant regardless of the angle. Then, the optimal wavelength for measuring all Bragg peaks is the same. However, the optimal angle will be different for each hkl .

Multiplying the flux for the decoupled hydrogen moderator by λ^2 at each wavelength gives the curve shown in Figure 11. From Figure 11, it is clear that wavelengths of about 1.5 to 6.0 Å provide the most effective flux. For an instrument length of 24.5 m, the wavelength band width is about 2.69 Å and hence neutrons with wavelength in the above region can be selected by using band width choppers.

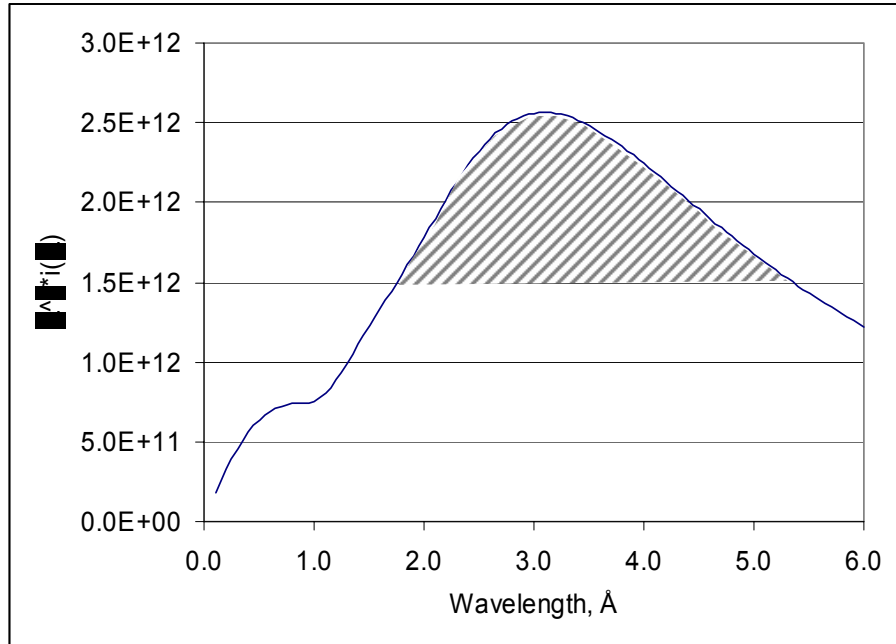


Figure 11. Plot of $\lambda^2 \cdot \phi(\lambda)$, n·Å/ster/pulse, versus wavelength for the decoupled, poisoned hydrogen moderator.

7) RESOLUTION

Table 6 provides parameters for the MANDI instrument for the calculation to resolve a d_{\min} of 1.5 Å for a unit cell repeat of 150 Å. Values for the angular dispersion are shown in Table 6 for the case where there are no guides and there is a full view of the moderator from the sample position. The total angular width for a crystal with a mosaic spread in this example is about $\Delta\theta = 0.3^\circ$.

Table 6. Parameters that determine the resolution of MANDI

Parameter	Value	Units
a axis	150	Å
d_{\min}	1.5	Å
$\Delta d/d$	0.01	
Required R (FWHM)	0.00469	
Initial Flight Path	24	M
Secondary Flight Path	0.5	M
Total Flight Path	24.5	M
Moderator width	0.1	M
Crystal size	0.001	M
Detector pixel size	0.001	M
Crystal mosaic	0.005	Rad
ΔL	0.02	M

Table 7. Parameters that determine angular resolution**Angular dispersion:**

Moderator to crystal position	0.004167	rad
Crystal to moderator position	0.000042	rad
Crystal to detector position	0.002000	rad
Detector pixel to crystal position	0.002000	rad
Crystal mosaic	0.005000	rad
$\Delta 2\theta$	0.007097	rad
$\Delta\theta$	0.003548	rad
	0.203305	deg

The FWHM Δt values for the hydrogen decoupled moderator (TU11) were obtained by fitting a second order polynomial to the shape metrics data in the file on the SNS moderators web page, and then multiplying by 1.6, as tabulated in Table 4.

The resolution at different scattering angles is shown in Table 8. Based on the R values, the actual d_{\min} where peaks are still resolvable for $a = 150 \text{ Å}$ is $d_{\min} = 2.3aR = 2.3 \cdot 150 \cdot R$ is shown in the column “ d_{\min} ($a=150 \text{ Å}$).” Alternatively, we can calculate the maximum lattice constant a for which peaks can be resolved at $d_{\min} = 1.5 \text{ Å}$. That is $a = d_{\min}/(2.3R) = 1.5/(2.3R)$ as shown in column “ a ($d_{\min}=1.5 \text{ Å}$).”

Table 8. Resolution of MANDI at different scattering angles.

Resolution R	2 θ	d_{\min} ($a=150$ Å)	a ($d_{\min} = 1.5$ Å)
0.01277	30	4.08	55.1
0.00614	60	1.96	114.7
0.00392	90	1.25	179.5
0.00290	120	0.93	242.4
0.00244	150	0.78	288.4

A plot of the resolvable d_{\min} vs. scattering angle for $a = 150$ Å is shown in Figure 12. This plot indicates that we can resolve peaks at $d_{\min} = 1.5$ Å for $a = 150$ Å at angles of about 75° and above. Most of the data would be obtained at from around 90° to higher backscattering angles. It is clear from Table 8 that there is a good wavelength match with the cold moderator. Thus MANDI will be using minimum wavelengths beginning with about 2.0 Å.

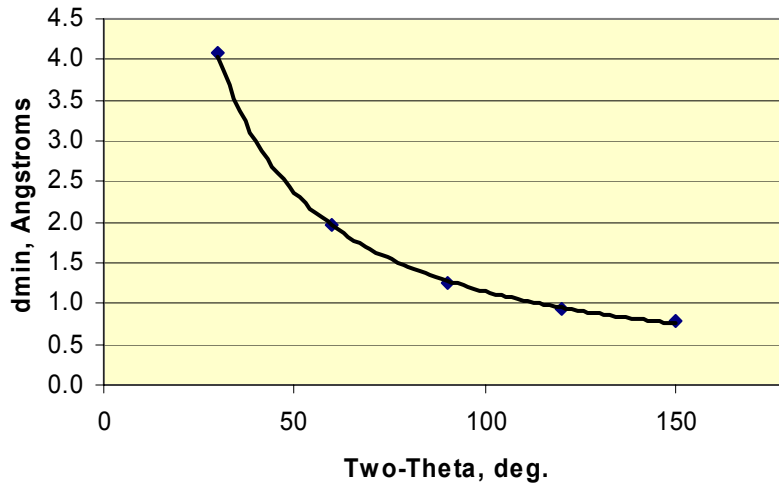


Figure 12. The resolvable d_{\min} vs. scattering angle for $a = 150$ Å.

8) DESIGN CALCULATIONS USING MC SIMULATIONS

We have carried out Monte Carlo (MC) simulations using the IDEAS⁵⁸ software package to determine the flux and divergence of the neutron beam at the sample position as a function of wavelength for various instrument configurations. MANDI will use high index state-of-the-art supermirror guides for efficient transport of cold neutrons. Neutron guides offer three advantages:

- Neutron guides with a width and height of 1.5 cm offer significant gains in flux when compared to natural collimation viewing the whole moderator.
- Curved guides in the middle section of the beam line make it possible to gently steer the neutron beam such that the sample is completely out of line-of-sight of the source.

Small widths of the beam allow for the more efficient operation of bandwidth choppers for wavelength selection. We have examined the length, location, curvature, type of supermirror coating, and the distance from the guide exit to the sample and determined the flux and divergence of the beam for different lengths of the instrument. MC calculations show that a gently curved guide in fact performs only marginally worse compared to a straight version of the same guide. A curved guide provides two distinct advantages: (1) It has a clear cut-off wavelength, i.e., it prevents leakage of short wavelength neutrons through absorbing beam conditioning devices (chopper blades, slits etc.); and (2) It will make the operation of MANDI easier from the safety point of view because it will allow only cold neutrons in the beam at the sample position. If a straight guide and a T_0 chopper were to be used, safety could not be assured because of possible T_0 chopper failure. That would also require building a more massive secondary shutter (to make the instrument operation independent of POW-GEN3), and all shielding would have to be based on the worst case scenario in which the T_0 chopper might fail.

Figure 13 shows the MC simulations of the flux and divergence of the neutron beam at the sample position. Corresponding divergences of the beam and the guide gains are given in Figures 14 and 15, respectively. It is clear from Figure 13 that substantial gain in flux can be achieved by using guides when compared to that employing natural collimation. Increase in the index of supermirror coating (m) increases the flux in the short wavelength region. The gain in intensity is related to the increase in the angular divergence of the beam as seen in Figure 14. It is important to note that the increase in divergence can be exploited to match the resolution requirements of a given experiment. The ratio of the intensity values with and without guides as a function of wavelength is plotted in Figure 15. Gains up to 10X can be achieved with guides.

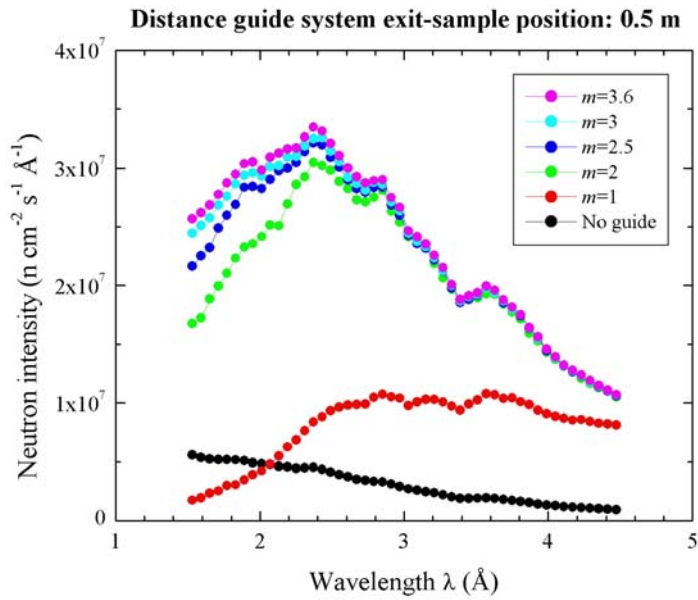


Figure 13. MC simulations of neutron intensity vs. wavelength for a 24.5 m long instrument without and with guides of various supermirror coatings.

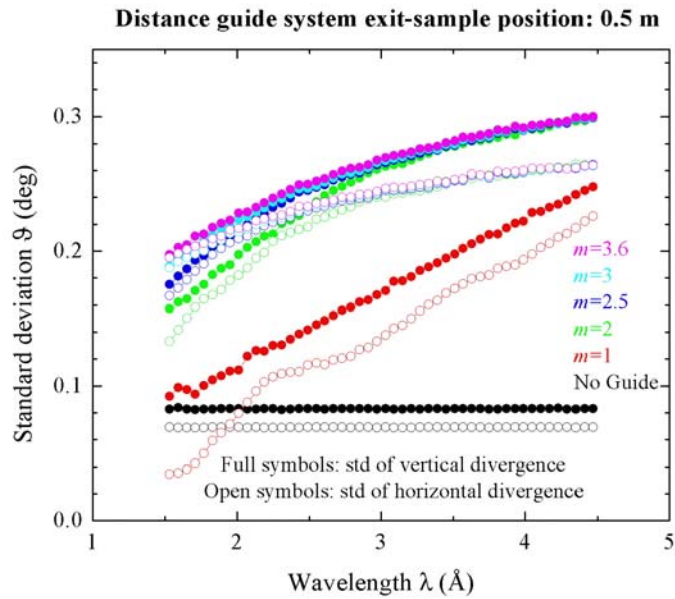


Figure 14. MC simulations of angular divergence vs. wavelength for a 24.5 m long instrument without and with guides of various supermirror coatings.

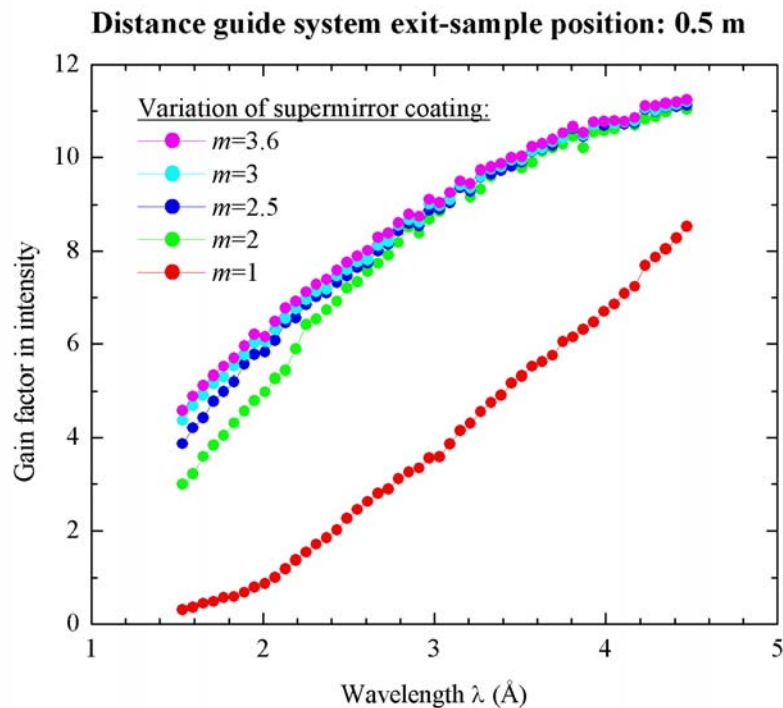


Figure 15. Flux gain factor due to guides compared to the natural collimation as a function of wavelength for a 24.5 m long instrument for various supermirror coatings.

9) BEAM DEFINING OPTICS AT THE SAMPLE

A variety of beam defining optics, such as Soller collimators, polycapillary focusing optics,⁵⁹ tapered guides and pin hole collimators, will be inserted between the guide exit and the sample to optimize the beam divergence to experimental requirements. Such flexibility will not be possible without the use of neutron guides.

10) DETECTORS

An array of position sensitive state-of-the-art area detectors with a spatial resolution of 1 mm will be used to cover a wide solid angle around the sample. New detector technology being developed at IPNS will enable the use of tiled area detectors with minimal gaps.

11) EXPECTED PERFORMANCE OF MANDI

A comparison of actual data collection times using neutron image plate instruments at reactor sources is given by Niimura and coworkers.⁶⁰ They present tables comparing BIX-3, using a monochromatic crystal rotating technique, with LADI, using a quasi-Laue technique. Selected portions of the tables are given below in Table 9.

Table 9. Reactor neutron image plate instruments

Instrument	BIX-3 (JAERI)	LADI (ILL)
Diffraction principle	Monochromatic	Quasi-Laue
Intensity, $\text{n s}^{-1} \text{cm}^{-2}$	3×10^6 ($\Delta\lambda/\lambda = 0.015$)	3×10^7 ($\Delta\lambda/\lambda = 0.28$ at 3.5 \AA)
Sample	Myoglobin	hew-lysozyme
Space group	Monoclinic $P2_1$	Tetragonal $P4_32_12$
$A, \text{ \AA}$	64.5	79.14
$B, \text{ \AA}$	30.9	79.14
$C, \text{ \AA}$	34.8	38.02
$\beta, ^\circ$	105.8	90
$V, \text{ \AA}^3$	67,000	145,000
$d_{\min}, \text{ \AA}$	1.5	2.0
$V_s, \text{ mm}^3$	6	6
Signal-to-noise ratio	10	1 (as a unit)
Exposure time per frame	~ 25 min	12 to 24 h
Number of frames	999	15
Data collection time, days	22	10

If we select a wavelength of $\lambda = 2.55 \text{ \AA}$, which is about the middle of the optimal wavelength range for the proposed instrument at SNS, then from the data file “source_sct091_tu_11_1.dat” provided by Iverson⁶¹ for the decoupled hydrogen moderator, we get

$$i(\lambda) = 3.8 \times 10^{11} \text{ n ster}^{-1} \text{ pulse}^{-1} \text{ \AA}^{-1} \quad (10)$$

Multiplying by 60 pulses/sec,

$$i(\lambda) = 2.3 \times 10^{13} \text{ n ster}^{-1} \text{ s}^{-1} \text{ \AA}^{-1} \quad (11)$$

For an incident path length of 24.5 m, we divide by $(2450 \text{ cm})^2$ to obtain the flux on sample at 2.55 \AA,

$$i(\lambda) = 3.8 \times 10^6 \text{ n cm}^{-2} \text{ s}^{-1} \text{ \AA}^{-1} \quad (12)$$

Multiplying by $\Delta\lambda = 4.4 - 1.71 = 2.69 \text{ \AA}$,

$$I_{INT} = i(\lambda)\Delta\lambda = 1.0 \times 10^7 \text{ n cm}^{-2} \text{ s}^{-1} \quad (13)$$

This is very close to the value of $7.62 \times 10^6 \text{ n cm}^{-2} \text{ s}^{-1}$ obtained from MC simulations for no guide. For the case of a curved/straight guide combination ending at 0.5 m upstream from the sample, the integrated intensity is $6.13 \times 10^7 \text{ n cm}^{-2} \text{ s}^{-1}$, which is 20 times greater than BIX-3.

The overall ratio of SNS to BIX-3 data collection rate is

$$\frac{SNS}{BIX3} = \left(\frac{I_{INT}(SNS)}{I_{INT}(BIX3)} \right) \left(\frac{\Delta\lambda(BIX3)}{\Delta\lambda(SNS)} \right) \left(\frac{\Delta v^*(SNS)}{\Delta v^*(BIX3)} \right) \quad (14)$$

where $\Delta v^* = (4/3)\pi[(1/\lambda_{min})^3 - (1/\lambda_{max})^3]$. Substituting the corresponding values, we obtain

$$\begin{aligned} \frac{SNS}{BIX3} &= \left(\frac{6.13 \times 10^7}{3 \times 10^6} \right) \left(\frac{0.035}{2.69} \right) \left(\frac{1.09}{0.0142} \right) \\ \frac{SNS}{BIX3} &= (20.4)(0.013)(79) \\ \frac{SNS}{BIX3} &= 21 \end{aligned}$$

For SNS this corresponds to an incident angular divergence *FWHM* of $\sim 0.25^\circ$ whereas the value for BIX-3 is about 0.4° due to the use of an elastically bent monochromator.⁶² By moving the end of the guide closer to the sample, the angular divergence of the SNS instrument can be made to match that of the BIX-3 instrument. This would lead to an increase in flux by about a factor of 2.5, such that the overall SNS data collection time would be about 50 times less than that for BIX-3.

The LADI instrument has a higher overall wavelength bandwidth and integrated flux in comparison to BIX-3, but with a substantial reduction in the signal-to-noise ratio. Niimura and coworkers⁶⁰ estimate that the signal-to-noise ratio differs by a factor of 10 between BIX-3 and LADI. With time-of-flight diffraction, the signal-to-noise for the SNS instrument will be similar to BIX-3 in principle.

12) POLARIZATION OPTICS FOR BACKGROUND REDUCTION

Using a polarized beam and a ^3He spin analyzing system, it is possible to significantly lower the spin-incoherent background signal.⁶³ Spin incoherent scattering is 1/3 non-spin flip and 2/3 spin flip. In principle, then, we should be able to filter out 2/3 of the incoherent background. The exact filtering efficiency depends on various factors such as beam polarization, multiple scattering effects, etc.

Since MANDI employs a cold neutron beam with quite small divergence, it can use a stacked supermirror polarizer and a spin flipper upstream to the sample to produce polarized neutrons, and a ^3He analyzer downstream from the sample.

13) PRELIMINARY BUDGET

The cost of building the MANDI instrument is about \$10 M. This figure has been reached based on the cost of various components, shielding, detectors and labor budgeted for other diffractometers at SNS.

14) REFERENCES

- (1) Tsyba, I.; Bau, R. *Chemtracts-Inorganic Chemistry* **2002**, *15*, 233-257.
- (2) Schoenborn, B. P. In *Nature in Biology, Basic Life Sciences*; Schoenborn, B. P., Ed.; Plenum Press: New York, 1984; Vol. 27, pp 261-281.
- (3) Schoenborn, B. P. *Methods Enzymol.* **1985**, *114*, 510.
- (4) Schoenborn, B. P. In *Neutrons in Biology, Basic Life Sciences*; Schoenborn, B. P.; Knott, R. B., Eds.; Plenum Press: New York, 1996; Vol. 64, pp 1-16.
- (5) Kossiakoff, A. A. *Annu. Rev. Biophys. Bioeng.* **1983**, *12*, 159.
- (6) Kossiakoff, A. A. *Basic Life Sci.* **1984**, *27*, 281.
- (7) Kossiakoff, A. A. *Annu. Rev. Biochem.* **1985**, *54*, 1195.
- (8) Wlodawer, A. *Prog. Biophys. Mol. Biol.* **1982**, *40*, 115.
- (9) Raghavan, N. V.; Wlodawer, A. *Methods Exp. Phys. Part C* **1987**, *23*, 335.
- (10) Timmins, P. A. *Physica B* **1995**, *213-214*, 26.

- (11) Helliwell, J. R. *Nature Struct. Biol.* **1997**, *11*, 874.
- (12) Niimura, N. *Curr. Op. Struct. Biol.* **1999**, *9*, 602.
- (13) Gutberlet, T.; Heinemann, U.; Steiner, M. *Acta Cryst. D* **2001**, *D57*, 349.
- (14) Shu, F.; Ramakrishnan, V.; Schoenborn, B. P. *Proc. Natl. Acad. Sci. USA* **2000**, *97*, 3872.
- (15) Coates, L.; Erskine, P. T.; Wood, S. P.; Myles, D. A. A.; Cooper, J. B. *Biochemistry* **2001**, *40*, 13149.
- (16) Niimura, N.; Minezaki, Y.; Nonaka, T.; Castagna, J. C.; Cipriani, F.; Hoeghøj, P.; Lehmann, M. S.; Wilkinson, C. *Nat. Struct. Biol.* **1997**, *4*, 909.
- (17) Ostermann, A.; Tanaka, I.; Engler, N.; Niimura, N.; Parak, F. G. *Biophys. Chem* **2002**, *95*, 183.
- (18) Bon, C.; Lehmann, M. S.; Wilkinson, C. *Acta Cryst. D* **1999**, *55*, 978-987.
- (19) Wlodawer, A.; Hendrickson, W. A. *Acta Crystallogr.* **1982**, *A38*, 239-247.
- (20) Wlodawer, A.; Walter, J.; Huber, R.; Sjölin, L. J. *J. Mol. Biol.* **1984**, *180*, 301-329.
- (21) Borah, B.; Chen, C. W.; Egan, W.; Miller, M.; Wlodawer, A.; Cohen, J. S. *Biochemistry* **1985**, *24*, 2058.
- (22) Wlodawer, A.; Savage, H.; Dodson, G. *Acta Crystallogr.* **1989**, *B45*, 99.
- (23) Habash, J.; Raftery, J.; Nuttall, R.; Price, H. J.; Wilkinson, C.; (Gilboa), A. J. K.; Helliwell, J. R. *Acta Cryst. D* **2000**, *56*, 541-550.
- (24) Deacon, A.; Gleichmann, T.; Kalb (Gilboa), A. J.; Price, H.; Raftery, J.; Bradbrook, G.; Yariv, J.; Helliwell, J. R. *J. Chem. Soc. Faraday Trans.* **1997**, *93*, 4305-4312.
- (25) Cooper, J. B.; Myles, D. A. A. *Acta Cryst. D* **2000**, *56*, 246-248.
- (26) Saenger, W.; Steiner, T. *Acta Cryst.* **1998**, *A54*, 798-805.
- (27) Mesecar, A. D.; Koshland, D. E., Jr. *IUBMB Life* **2000**, *49*, 457-466.
- (28) Mesecar, A. D.; Koshland, D. E., Jr. *Nature* **2000**, *403*, 614-615.
- (29) Stoddard, B. L.; Cohen, B. E.; Brubaker, M.; Mesecar, A. D.; Koshland, D. E., Jr. *Nat Struct Biol* **1998**, *5*, 891-897.

- (30) Mesecar, A. D.; Stoddard, B. L.; Koshland, D. E., Jr. *Science* **1997**, *277*, 202-206.
- (31) Larsen, T. M.; Wedekind, J. E.; Rayment, I.; Reed, G. H. *Biochemistry* **1996**, *35*, 4349-4358.
- (32) Desmarais, W. T.; Bienvenue, D. L.; Bzymek, K. P.; Holz, R. C.; Petsko, G. A.; Ringe, D. *Structure (Camb)* **2002**, *10*, 1063-1072.
- (33) Rubach, J. K.; Plapp, B. V. *Biochemistry* **2003**, *42*, 1178.
- (34) Rubach, J. K.; Plapp, B. V. *Biochemistry* **2003**, *42*, 2907-2915.
- (35) Minasov, G.; Wang, X.; Shoichet, B. K. *J Am Chem Soc* **2002**, *124*, 5333-5340.
- (36) Pokkuluri, P. R.; Laible, P. D.; Deng, Y.-L.; Wong, T. N.; Hanson, D. K.; Schiffer, M. *Biochemistry* **2002**, *41*, 5998-6007.
- (37) Mukherjee, M.; Maiti, S.; Ghosh, S.; Woolfson, M. M. *Acta Cryst.* **2001**, *D57*, 1276-1280.
- (38) Durley, R.; Chen, L.; Lim, L. W.; Mathews, F. S.; Davidson, V. L. *Protein Sci.* **1993**, *2*, 739-752.
- (39) Chen, Z. W.; Barber, M. J.; McIntire, W. S.; Mathews, F. S. *Acta Cryst.*, *D54*, 253-268.
- (40) Pirrung, M. C.; Han, Y.; Chen, J. *J. Org. Chem.* **1996**, *61*, 4527-4531.
- (41) Bolduc, J. M.; Dyer, D. H.; Scott, W. G.; Singer, P.; Sweet, R. M.; D.E. Koshland, J.; Stoddard, B. L. *Science* **1995**, *268*, 1312-1318.
- (42) Stoddard, B. L.; Dean, A.; Bash, P. A. *Nat. Struct. Biol.*, *3*, 590-595.
- (43) Rose, I. A.; O'Connell, E. L.; Mortlock, R. P. *Biochem. Biophys. Acta* **1969**, *178*, 376-379.
- (44) Farber, G. K.; Glasfeld, A.; Tiraby, G.; Ringe, D.; Petsko, G. A. *Biochemistry* **1989**, *28*, 7289-7297.
- (45) Collyer, C. A.; Henrick, K.; Blow, D. M. *J. Mol. Biol.* **1990**, *212*, 211-235.
- (46) Whitlow, M.; Howard, A. J.; Finzel, B. C.; Poulos, T. L.; Winborne, E.; Gilliland, G. L. *Proteins Struct. Funct. Genet.* **1991**, *9*, 153-173.
- (47) Lavie, A.; Allen, K. N.; Petsko, G. A.; Ringe, D. *Biochemistry* **1994**, *33*, 5469-5480.
- (48) Carrell, H. L.; Hoier, H.; Glusker, J. P. *Acta Cryst.* **1994**, *D50*, 113-123.

- (49) Deisenhofer, J.; Epp, O.; Huber, R.; Michel, H. *Nature* **1985**, *318*, 618-624.
- (50) Sebban, P.; Maróti, P.; Hanson, D. K. *Biochimie* **1995**, *77*, 677-694.
- (51) Okamura, M. Y.; Paddock, M. L.; Graige, M. S.; Feher, G. *Biochim. Biophys. Acta* **2000**, *1458*, 148-163.
- (52) Paddock, M. L.; Feher, G.; Okamura, M. Y. *Proc. Natl. Acad. Sci. USA* **2000**, *97*, 1548-1553.
- (53) Axelrod, H. L.; Abresch, E. C.; Paddock, M. L.; Okamura, M. Y.; Feher, G. *Proc. Natl. Acad. Sci. USA* **2000**, *97*, 1542-1547.
- (54) Ädelroth, P.; Paddock, M. L.; Sagle, L. B.; Feher, G.; Okamura, M. Y. *Proc. Natl. Acad. Sci. USA* **2000**, *97*, 13086-13091.
- (55) Niimura, N.; Minezaki, Y.; Nonaka, T.; Castagna, J. C.; Cipriani, F.; Hoghoj, P.; Lehmann, M. S.; Wilkinson, C. *Nat Struct Biol* **1997**, *4*, 909-914.
- (56) Jauch, W. *Transactions ACA* **1993**, *29*, 55-61.
- (57) Jauch, W. In *ISIS Workshop*: Rapallo, Italy, 1986.
- (58) Lee, W.-T.; Wang, X.-L. *Neutron News* **2002**, *13*, 30-34.
- (59) Gibson, W. M.; Schultz, A. J.; Chen-Mayer, H. H.; Mildner, D. F. R.; Gnaupel-Herold, T.; Miller, M. E.; Prasad, H. J.; Youngman, R.; Carpenter, J. M. *J. Applied Cryst.* **2002**, *35*, 677-683.
- (60) Tanaka, I.; Kurihara, K.; Chatake, T.; Niimura, N. *J. Appl. Cryst.* **2002**, *35*, 34-40.
- (61) Iverson, E. B., 2002.
- (62) Ahmed, F. U.; Tanaka, I.; Niimura, N. *J. Apply. Cryst.* **2000**, *33*, 291-295.
- (63) Gentile, T. R.; Jones, G. L.; K.Thompson, A.; Barker, J.; Glinka, C. J.; Hammouda, B.; Lynn, J. W. *J. Appl. Cryst.* **2000**, *33*, 771-774.

15) IDT MEMBERS AND THEIR AFFILIATION

Robert Bau	University of Southern California
Jeffrey Bolin	Purdue University
Gerry Bunick	Oak Ridge National Laboratory
Dan Carter	New Century Pharmaceuticals, Inc.
V.L. Davidson	University of Mississippi, Jackson
Chris Dealwis	University of Tennessee, Knoxville
Leif Hanson	University of Tennessee, Knoxville
Deborah K. Hanson	Argonne National Laboratory
Chuan He	University of Chicago
Jason Hodges	Spallation Neutron Source
Thomas Koetzle	Brookhaven National Laboratory/Argonne National Laboratory
P. Laible	Argonne National Laboratory
Paul Langan	Los Alamos National Laboratory
F. Scott Mathews	Washington University School of Medicine, St. Louis
Andrew Mesecar	University of Illinois, Chicago
Greg Petsko	Brandeis University
Bryce V. Plapp	University of Iowa
R. Pokkaluri	Argonne National Laboratory
S. Ramaswamy	University of Iowa
Christine Rehm	Spallation Neutron Source
Dagmar Ringe	Brandeis University
Bernie Santarsiero	University of Illinois, Chicago
Benno Schoenborn	Los Alamos National Laboratory
Arthur Schultz	Argonne National Laboratory
Brian Shoichet	Northwestern University
Barry Stoddard	Fred Hutchinson Cancer Research Center
Vukica Srajer	BioCARS Associate Project Manager
N. Sukumar	Cornell University
P. Thiyagarajan	Argonne National Laboratory
J.K. Zhou	Spallation Neutron Source